Supporting Information: The π-Interactions of Ammonia Ligands Evaluated by *ab initio* Ligand Field Theory

Moritz Buchhorn[1] and Prof. Dr. Vera Krewald[1*]

[1]TU Darmstadt, Department of Chemistry, Theoretical Chemistry, Alarich-Weiss-Straße 4, 64287 Darmstadt, Germany
[*]vera.krewald@tu-darmstadt.de

Contents

List of Figures

List of Tables

1 A few comments on d-s mixing

In the Introduction, Fig. 1, we labelled the d_{z^2} orbital energy with a d-s mixing contribution. d-s mixing generally needs to be considered if at least one d orbital transforms in the totally symmetric irreducible representation of the molecular point group. It is best known in square planar complexes, but also the elongated octahedron and the square pyramid have d-s mixing contributions to the d_{z^2} orbital energy:

$$\begin{aligned} \text{elong.oct.} \quad & \Delta_{ds}\varepsilon_{z^2} = -(2e_{ds,ax} - 2e_{ds,eq})^2 \\ \text{sq.pyr.} \quad & \Delta_{ds}\varepsilon_{z^2} = -(e_{ds,ax} - 2e_{ds,eq})^2 \end{aligned}$$

Deeth, Gerloch and Woolley showed that in the square planar case, the introduction of d-s mixing is equivalent to placing σ-only pseudo ligands on the z-axis, termed coordination voids. These voids then have negative e_σ parameters and account for the lower d_{z^2} orbital energy. Consequently, an elongated octahedron automatically covers the effect of d-s mixing by having a reduced e_σ for the axial ligands and one may drop the d-s mixing term.

2 Influence of implicit solvation models

As stated in the methodology section, we do not employ solvation models for our CASSCF calculations. Tests with and without solvation yield roughly the same AOM parameters at higher computational costs. The difference between the parameters is less than $100\,cm^{-1}$ and all trends are the same. Another effect of implicit solvation is a change in some orbital energies for complexes with empty

coordination sites. For square planar complexes, the d_{z^2} orbital energy increases significantly when implicit solvation is included. The empty sites are covered by the polarizable solvent surface and act similar to an additional ligand. This is an undesired effect when comparing with the experimental crystal structure data.

For geometry optimizations of complexes of the type $[MCl_6]^{3/4-}$, the inclusion of an implicit solvation model is necessary because of the large negative charge. Without a solvation model, the charge leads the ligands to repel each other, leading to asymmetric structures, if convergence is achieved at all. The CASSCF calculations are still conducted without a solvation model.

3 Square pyramidal copper pentammine

The experimental structure of the $Cu(NH_3)_5$ unit is roughly square pyramidal, with the structural parameters given in Table 1. Assuming a perfect square pyramid (C_{4v}), we obtain the following AOM parameterization for V_{LF}:

$$V_{LF} = \begin{bmatrix} 4.0e_\pi & 0 & 0 & 0 & 0 \\ 0 & 3.0e_\pi & 0 & 0 & 0 \\ 0 & 0 & 2.0e_\sigma - 1.0e_{ds} & 0 & 0 \\ 0 & 0 & 0 & 3.0e_\pi & 0 \\ 0 & 0 & 0 & 0 & 3.0e_\sigma \end{bmatrix}$$

which directly yields the following eigenvalues on the diagonal:

$$\begin{aligned} E_{d_{xy}} &= 4.0e_\pi \\ E_{d_{yz}} &= 3.0e_\pi \\ E_{d_{z^2}} &= 2.0e_\sigma - 1.0e_{ds} \\ E_{d_{xz}} &= 3.0e_\pi \\ E_{d_{x^2-y^2}} &= 3.0e_\sigma \end{aligned}$$

It is apparent that the energy difference between the d_{yz}/d_{xz} orbitals and the d_{xy} orbital is e_π. Plugging in the measured energy difference of $1300\,\mathrm{cm}^{-1}$, we obtain the same value for the π parameter.

The above calculation relies on a square pyramidal structure with right angles and equal bond lengths. When using the actual structure data in Table 1, we arrive at a different ligand field potential and the diagonalized matrix is much more complicated:

$$V_{LF} =$$
$$\begin{bmatrix} 3.93e_\pi & 0 & 0 & 0 & 0 \\ 0 & 2.88e_\pi + 0.113e_\sigma & 0 & 0 & 0 \\ 0 & 0 & -0.8e_{ds} + 0.207e_\pi + 1.897e_\sigma & 0 & 0.005e_{ds} + 0.011e_\pi - 0.011e_\sigma \\ 0 & 0 & 0 & 2.914e_\pi + 0.094e_\sigma & 0 \\ 0 & 0 & 0.005e_{ds} + 0.011e_\pi - 0.011e_\sigma & 0 & 0.069e_\pi + 2.895e_\sigma \end{bmatrix}$$

$$\begin{aligned} E_{d_{xy}} &= 3.93e_\pi \\ E_{d_{yz}} &= 2.88e_\pi + 0.113e_\sigma \\ E_{d_{z^2}} &= -0.4e_{ds} + 0.138e_\pi + 2.4e_\sigma \\ &\quad - 0.632\left(0.401e_{ds}^2 - 0.138e_{ds}e_\pi + e_{ds}e_\sigma + 0.0122e_\pi^2 - 0.173e_\pi e_\sigma + 0.624e_\sigma^2\right)^{0.5} \\ E_{d_{xz}} &= 2.91e_\pi + 0.0938e_\sigma \\ E_{d_{x^2-y^2}} &= -0.4e_{ds} + 0.138e_\pi + 2.4e_\sigma \\ &\quad + 0.632\left(0.401e_{ds}^2 - 0.138e_{ds}e_\pi + e_{ds}e_\sigma + 0.0122e_\pi^2 - 0.173e_\pi e_\sigma + 0.624e_\sigma^2\right)^{0.5} \end{aligned}$$

Even this is still a simplification, since we subsume the parameters of the first nitrogen atom with the ones of the other four nitrogen atoms. Without going into further detail, the orbital energy difference between d_{yz}/d_{xz} and d_{xy} is roughly $e_\pi - 0.1e_\sigma$, leading to a π parameter that is slightly larger than the measured energy gap of $1300\,\mathrm{cm}^{-1}$.

Table 1: Experimental bond lengths (Å) and angles (°) for $Cu(NH_3)_5$.

Bond lengths /Å	
Cu–N_1	2.19
Cu–N_2	2.01
Cu–N_3	2.01
Cu–N_4	2.05
Cu–N_5	2.05
Angles /°	
N_1–Cu–N_2	98
N_1–Cu–N_3	98
N_1–Cu–N_4	97
N_1–Cu–N_5	97
N_2–Cu–N_3	164
N_4–Cu–N_5	166

3.1 Influence of spin–orbit coupling

In $[Cu(NH_3)_5]^{2+}$, SOC only couples the states with singly occupied d_{xy}, d_{xz} and d_{yz} orbitals, and the spin–orbit coupled states have an energetic ordering

very similar to that of the uncoupled case.

Although the assignment is not as clear-cut as without SOC, we note that the energy difference between the second excited state (d_{xy} orbital contribution 68 %) and the fourth excited state (d_{xz} and d_{yz} orbital contribution 37 % and 59 %) can only be explained by an ammonia π interaction.

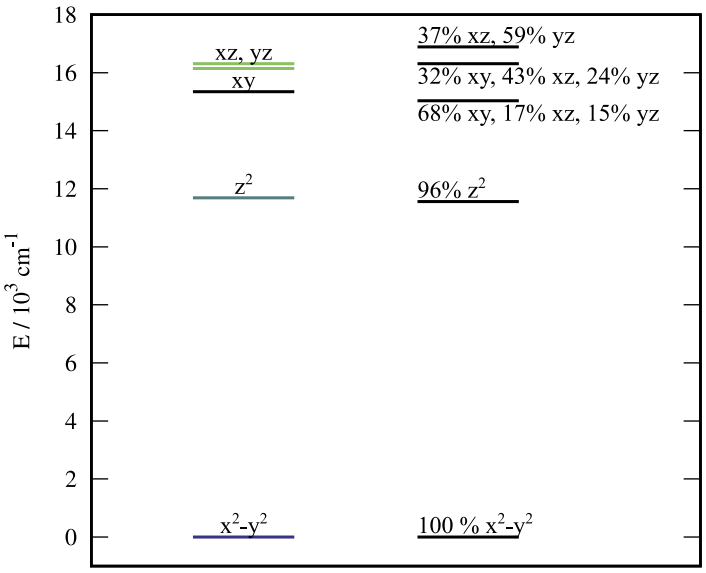

Figure 1: Energy levels of $[Cu(NH_3)_5]^{2+}$ with NEVPT2 correction (left) and upon consideration of spin–orbit coupling (right). Due to the coupling, the assignment of orbital occupations to electronic states is not as clear anymore.

Table 2: Electronic states of $[Cu(NH_3)_5]^{2+}$ and their orbital compositions with spin–orbit coupling. The configuration contribution is written in terms of the singly occupied orbital in the uncoupled contribution. Since the uncoupled states consist of (almost) a single configuration each, we use the orbital-based assignments also in the coupled states.

Energy / cm^{-1}	configuration contributions				
	d_{xy}	d_{yz}	d_{z^2}	d_{xz}	$d_{x^2-y^2}$
CASSCF					
0	0.00	0.00	0.00	0.00	0.99
8456	0.00	0.03	0.93	0.03	0.00
10305	0.73	0.13	0.00	0.13	0.00
11684	0.26	0.30	0.00	0.43	0.00
12374	0.00	0.54	0.07	0.39	0.00
CASSCF + NEVPT2					
0	0.00	0.00	0.00	0.00	1.00
11560	0.00	0.00	0.96	0.00	0.00
15032	0.68	0.15	0.00	0.17	0.00
16308	0.32	0.24	0.00	0.43	0.00
16892	0.00	0.59	0.03	0.37	0.00

4 Square planar copper tetrammine

Table 3: Experimental and calculated d-d transitions for $[Cu(NH_3)_4]^{2+}$.

	$E(B_{1g} \rightarrow A_{1g})$ / cm^{-1}	E($B_{1g} \rightarrow B_{2g}$) / cm^{-1}	$E(B_{1g} \rightarrow E_g)$ / cm^{-1}
CASSCF	14992 - 14995	12262	14990
NEVPT2	20617 - 20631	18055	20376
Experimental	13600 - 13700		17400 - 17800

Table 4: Calculated d-d transitions for square planar $[Cu(NH_3)_4]^{2+}$ with and without NEVPT2 correction and with different basis sets. The acceptor orbital in each transition is $d_{x^2-y^2}$, so only the donor orbital is given.

method	basis set	$d_{xz} \rightarrow$ /cm^{-1}	$d_{yz} \rightarrow$ /cm^{-1}	$d_{z^2} \rightarrow$ /cm^{-1}	$d_{xy} \rightarrow$ /cm^{-1}
CASSCF	def2-SVP	14964	14966	14890	12452
	def2-TZVP	14992	14995	14990	12262
	def2-QZVP	14959	14960	14981	12227
NEVPT2	def2-SVP	19832	19831	19543	17495
	def2-TZVP	20617	20631	20376	18055
	def2-QZVP	20463	20464	20177	17980

4.1 Influence of spin–orbit coupling

In $[Cu(NH_3)_4]^{2+}$, SOC only couples the states with singly occupied d_{z^2}, d_{xz} and d_{yz} orbitals, leading to four excited states with relatively small energy differences. It is apparent that the first excited state is still clearly dominated by a singly occupied d_{xy} orbital. Again, the energy difference between this and the higher excited states can only be explained with an ammonia π interaction.

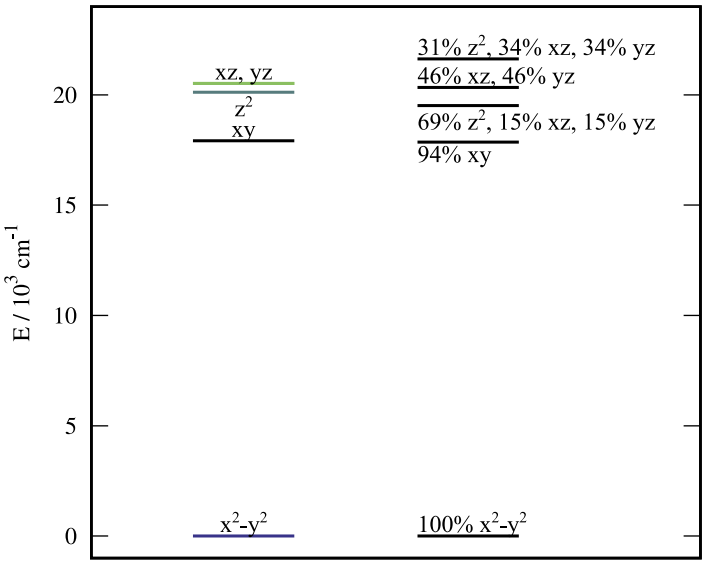

Figure 2: Energy levels of $[Cu(NH_3)_4]^{2+}$ with NEVPT2 correction (left) and upon consideration of spin–orbit coupling (right). Due to the coupling, the assignment of orbital occupations to electronic states is not as clear anymore.

Table 5: Electronic states of $[Cu(NH_3)_4]^{2+}$ and their orbital compositions with spin–orbit coupling. Configuration contribution is written in terms of the singly occupied orbital in the uncoupled contribution. Since the uncoupled states consist of (almost) a single configuration each, we convey the orbital assignments to the coupled states.

Energy / cm^{-1}	configuration contributions				
	d_{xy}	d_{yz}	d_{z^2}	d_{xz}	$d_{x^2-y^2}$
CASSCF					
0	0.00	0.00	0.00	0.00	0.99
12234	0.94	0.02	0.00	0.02	0.00
14203	0.00	0.19	0.61	0.19	0.00
14826	0.06	0.47	0.00	0.47	0.00
16232	0.00	0.31	0.38	0.31	0.00
CASSCF + NEVPT2					
0	0.00	0.00	0.00	0.00	1.00
17855	0.94	0.02	0.00	0.02	0.00
19514	0.00	0.15	0.69	0.15	0.00
20331	0.06	0.46	0.00	0.46	0.00
21636	0.00	0.34	0.31	0.34	0.00

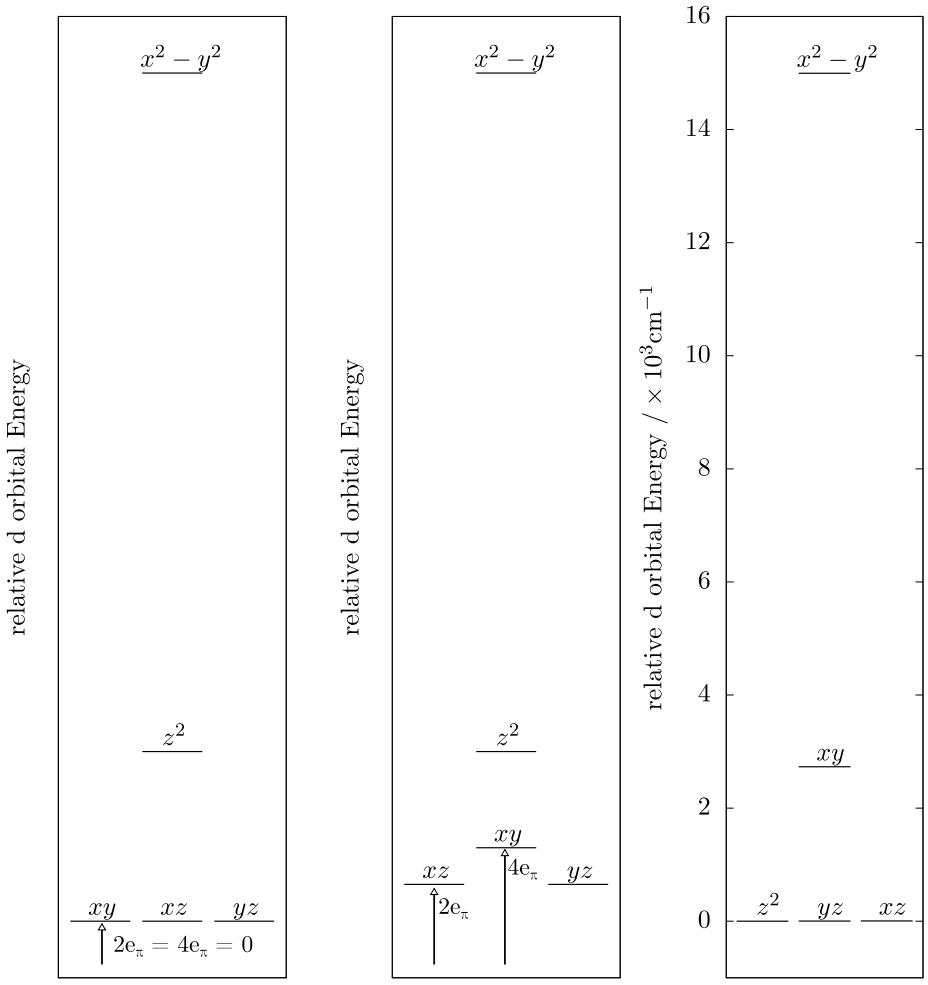

Figure 3: Expected d orbital energies for square planar complexes without π interaction (left), with π interaction (centre) and the energy levels for $[Cu(NH_3)_4]^{2+}$ from CASSCF calculations (right). The position of the z^2 orbital in the schemes on the left and centre is incompletely defined and depends on the parameter e_{ds}. It is noteworthy that the degeneracy in the left and right panel is no symmetry feature, as the d_{xz} and d_{yz} orbitals transform in the E_g representation of D_{4h}, while the d_{xy} and d_{z^2} orbital transform in the B_{2g} and A_{1g} representation, respectively.

5 Table data and plots for octahedral hexammines

It is apparent that some of the parameters (Cr^{2+}, intermediate spin Mn^{3+}, Ni^{3+}, i.e. chemically unrealistic or very challenging to obtain complexes) have uncom-

fortably large standard deviations, up to a level where the data point must be considered unreliable. The reason for the large scattering of parameters probably reflects the improbability of finding the compound in reality which poses a challenge for our procedure that may not be applicable to every hypothetical coordination compound. Nonetheless, most of the parameters have reasonable standard deviations that justify an interpretation, and ligand field splittings generally match expectations.

Table 6: AOM parameters for $[M(NH_3)_6]^{n+}$. Multiplicity refers to the multiplicity of the optimized ground state, ΔE is the energy difference to the ground state.

Complex	$2S+1$	ΔE/kJ mol^{-1}		bond length / Å	e_σ/cm^{-1}	e_π/cm^{-1}
$[Cr(NH_3)_6]^{2+}$	3	0	1	2.173(0.005)	6594(2760)	1527(2070)
$[Cr(NH_3)_6]^{3+}$	4	0	1	2.145(0.001)	6743(341)	1027(255)
$[Mn(NH_3)_6]^{2+}$	6	0	1	2.349(0.002)	3613(213)	894(159)
$[Mn(NH_3)_6]^{3+}$	3	5	1	2.099(0.003)	8917(4505)	2584(3378)
$[Mn(NH_3)_6]^{3+}$	5	0	ax	2.369(0.002)	3285(360)	576(270)
$[Mn(NH_3)_6]^{3+}$	5	0	eq	2.127(0.002)	6707(359)	1046(270)
$[Fe(NH_3)_6]^{2+}$	1	5	1	2.059(0.000)	5491(324)	710(243)
$[Fe(NH_3)_6]^{2+}$	3	43	ax	2.038(0.000)	6011(352)	1051(263)
$[Fe(NH_3)_6]^{2+}$	3	43	eq	2.250(0.016)	3772(385)	826(265)
$[Fe(NH_3)_6]^{2+}$	5	0	1	2.282(0.002)	3598(229)	851(171)
$[Fe(NH_3)_6]^{3+}$	6	56	1	2.237(0.003)	6532(915)	2052(683)
$[Fe(NH_3)_6]^{3+}$	4	47	ax	2.323(0.000)	3909(907)	972(679)
$[Fe(NH_3)_6]^{3+}$	4	47	eq	2.081(0.002)	7452(909)	1433(682)
$[Fe(NH_3)_6]^{3+}$	2	0	1	2.061(0.003)	7042(92)	1087(74)
$[Co(NH_3)_6]^{2+}$	4	0	1	2.233(0.008)	3471(62)	770(19)
$[Co(NH_3)_6]^{2+}$	2	7	ax	2.391(0.002)	1818(379)	591(284)
$[Co(NH_3)_6]^{2+}$	2	7	eq	2.022(0.000)	5857(379)	1024(285)
$[Co(NH_3)_6]^{3+}$	1	0	1	2.024(0.000)	6788(408)	698(307)
$[Ni(NH_3)_6]^{2+}$	3	0	1	2.182(0.000)	3024(355)	412(266)
$[Ni(NH_3)_6]^{3+}$	4	0	1	2.153(0.000)	7515(1628)	1971(1238)
$[Ni(NH_3)_6]^{3+}$	4	0	2	2.222(0.000)	6804(1058)	2665(792)
$[Ni(NH_3)_6]^{3+}$	4	0	3	2.181(0.000)	7500(1420)	2349(1060)
$[Ru(NH_3)_6]^{2+}$	1	0	1	2.164(0.003)	9755(203)	799(152)
$[Ru(NH_3)_6]^{3+}$	2	0	1	2.168(0.005)	10749(417)	649(311)
$[Os(NH_3)_6]^{2+}$	1	0	1	2.182(0.005)	11271(156)	594(120)
$[Os(NH_3)_6]^{3+}$	2	0	1	2.186(0.004)	11686(170)	194(149)

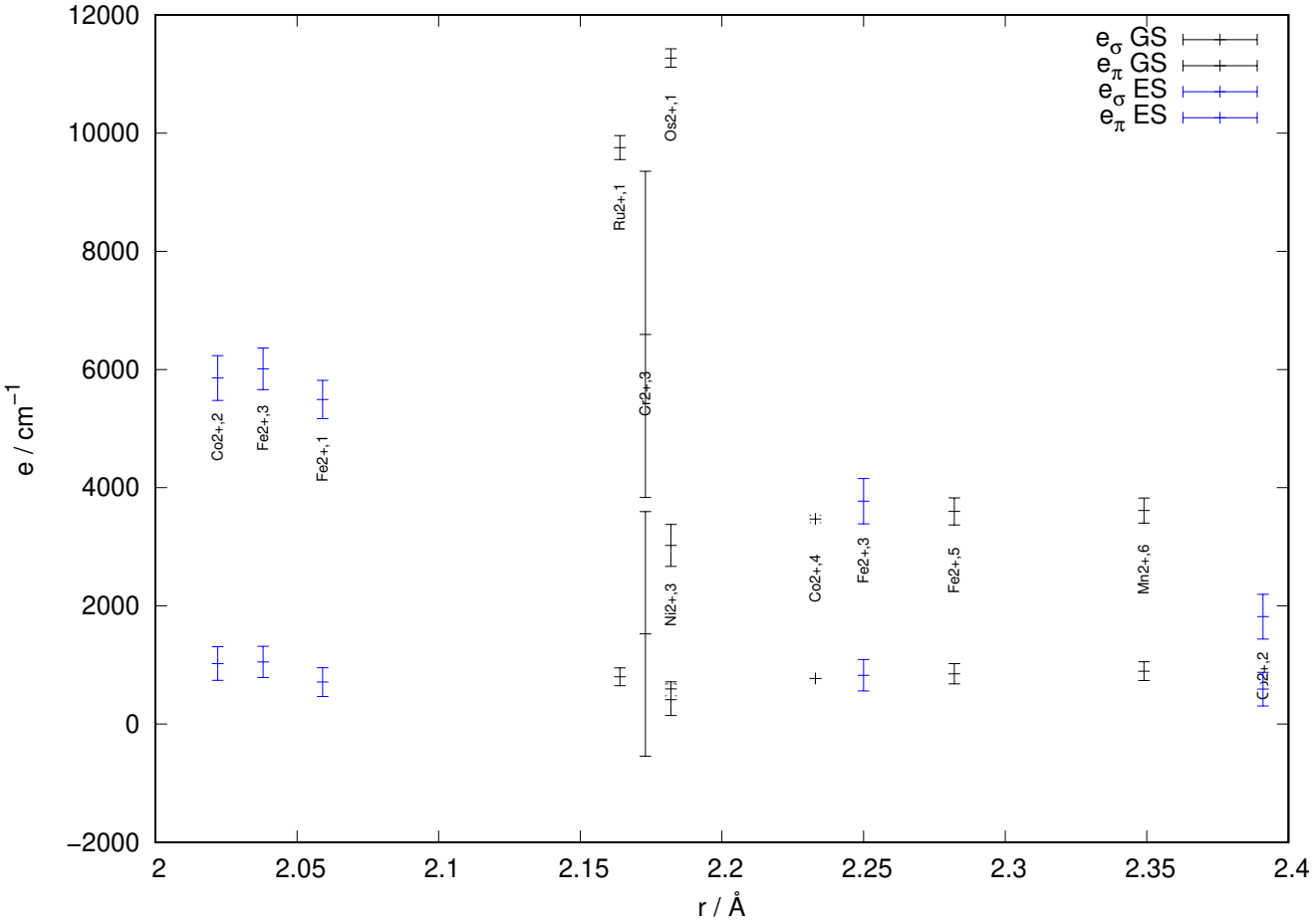

Figure 4: AOM parameters of M^{II} hexammine complexes plotted versus the corresponding bond length. The upper set of points represents σ parameters, the lower set of points π parameters. Data points of the ground spin state structures (GS) and of structures with less stabilised multiplicities (ES) are colored black and blue, respectively. The error bars show the standard deviations resulting from sampled calculations. Labels indicate the metal with formal charge and multiplicity.

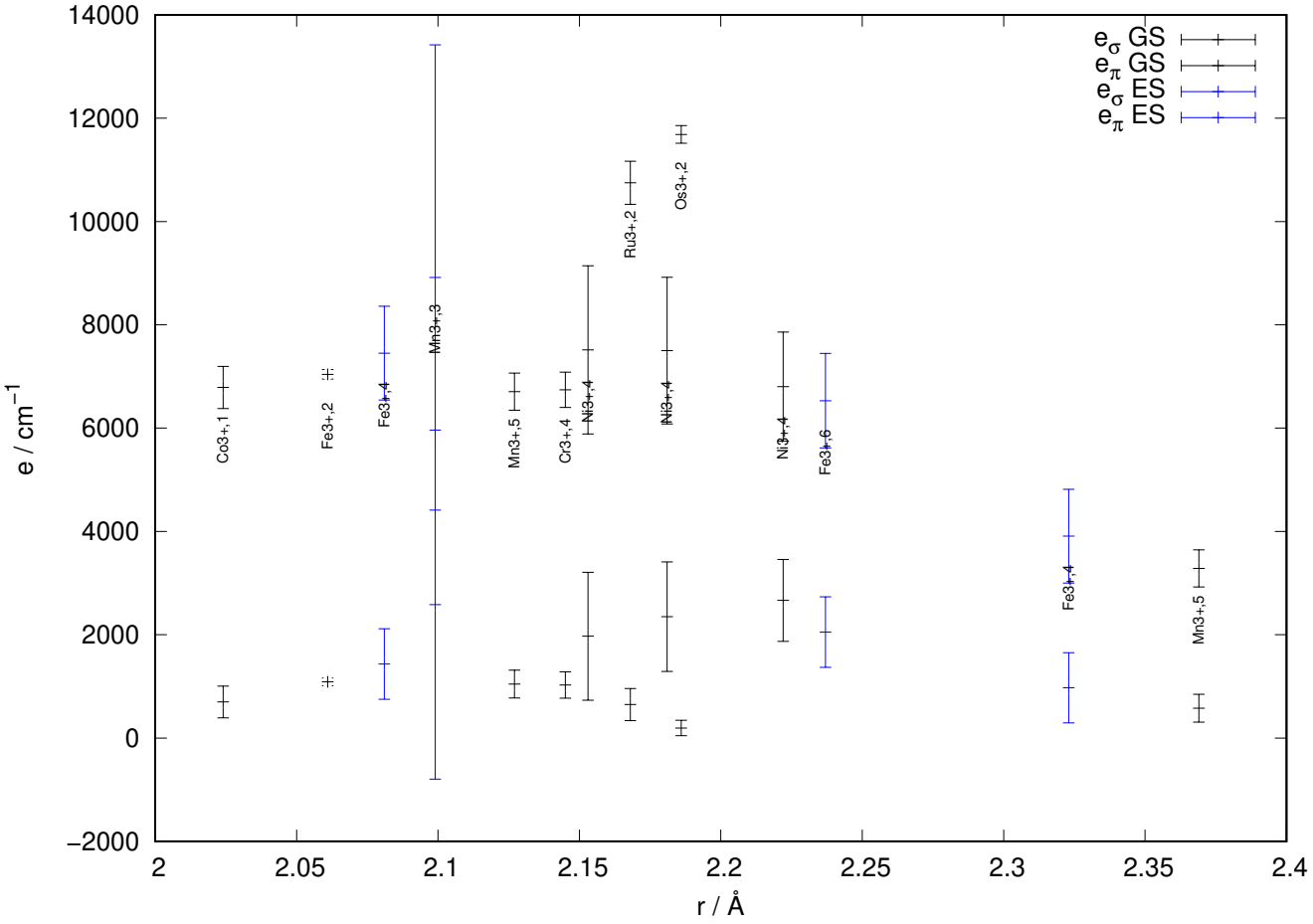

Figure 5: AOM parameters of M^{III} hexammine complexes plotted versus the corresponding bond length. The upper set of points represents σ parameters, the lower set of points π parameters. Data points of the ground spin state structures (GS) and of structures with less stabilised multiplicities (ES) are colored black and blue, respectively. The error bars show the standard deviations resulting from sampled calculations. Labels indicate the metal with formal charge and multiplicity.

6 Comparison of chloride and ammine ligands

For the parameters that do not have an overly large standard deviation, some patterns can be seen: Both σ and π parameters are larger for ammine ligands than for chloride ligands. Shorter bond lengths lead to higher σ parameters, but not necessarily to higher π parameters. Plotting the parameters of Cl^- ligands against the ones of NH_3 ligands shows absolutely no correlation. No rule in the sense of a parameter ratio can be derived from the calculations.

Table 7: AOM parameters for $[MCl_6]^{3-/4-}$, optimized with BP, def2-SVP, Grid5, CPCM(Water).

Complex	$2S+1$	ΔE/kJ mol^{-1}		bond length / Å	e_σ/cm^{-1}	e_π/cm^{-1}
$[CrCl_6]^{3-}$	4	0	1	2.410(04)	3987(72)	537(39)
$[MnCl_6]^{4-}$	6	0	1	2.639(05)	1930(31)	516(13)
$[MnCl_6]^{3-}$	3	0	1	2.376(04)	3892(110)	435(74)
$[FeCl_6]^{4-}$	5	0	ax	2.619(00)	1659(15)	410(11)
$[FeCl_6]^{4-}$	5	0	eq	2.583(02)	1836(18)	448(12)
$[FeCl_6]^{3-}$	6	0	1	2.454(08)	3363(86)	462(24)
$[CoCl_6]^{4-}$	4	0	1	2.529(02)	1928(22)	501(16)
$[CoCl_6]^{4-}$	4	0	2	2.635(00)	1416(21)	393(16)
$[CoCl_6]^{3-}$	1	2	1	2.329(05)	3975(67)	312(17)
$[CoCl_6]^{3-}$	5	0	1	2.437(04)	3425(52)	414(20)
$[CoCl_6]^{3-}$	3	19	ax	2.302(00)	4711(118)	606(88)
$[CoCl_6]^{3-}$	3	19	eq	2.436(16)	3087(211)	245(94)
$[NiCl_6]^{4-}$	3	0	ax	2.491(00)	1813(49)	430(37)
$[NiCl_6]^{4-}$	3	0	eq	2.553(04)	1517(52)	367(37)
$[NiCl_6]^{3-}$	2	0	ax	2.563(00)	1391(465)	-129(349)
$[NiCl_6]^{3-}$	2	0	eq	2.295(02)	4720(466)	423(349)
$[RuCl_6]^{4-}$	1	0	1	2.488(08)	4678(104)	378(19)
$[RuCl_6]^{3-}$	2	0	ax	2.441(00)	6236(143)	306(107)
$[RuCl_6]^{3-}$	2	0	eq	2.407(01)	6849(144)	404(107)
$[RuCl_6]^{3-}$	4	68	ax	2.679(00)	3068(547)	103(409)
$[RuCl_6]^{3-}$	4	68	eq	2.417(02)	7345(547)	742(410)
$[OsCl_6]^{4-}$	1	0	1	2.518(07)	5224(120)	256(55)
$[OsCl_6]^{3-}$	2	0	ax	2.468(00)	6903(216)	356(162)
$[OsCl_6]^{3-}$	2	0	eq	2.428(01)	7674(218)	457(162)

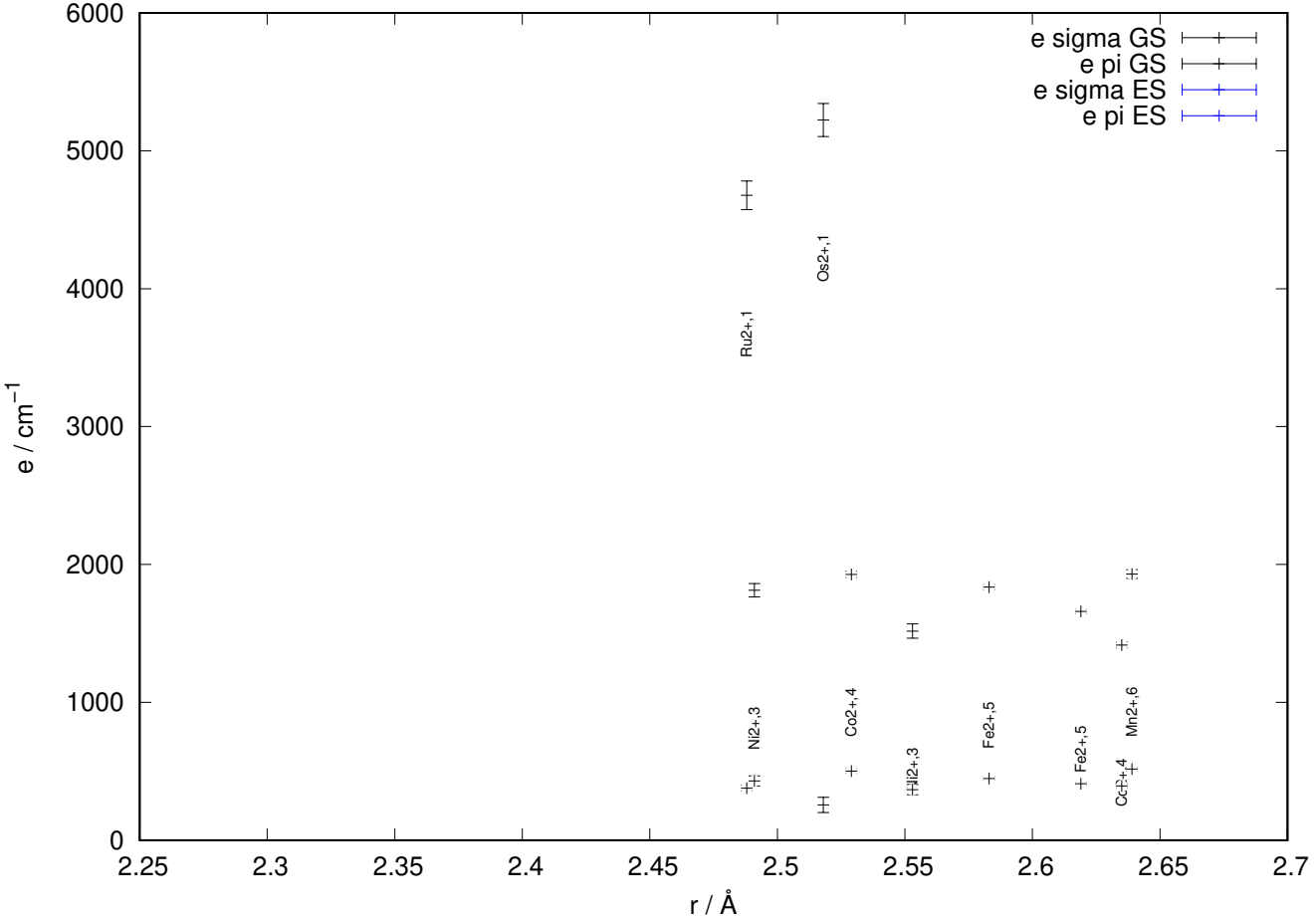

Figure 6: AOM parameters of M^{II} hexachloride complexes plotted versus the corresponding bond length. The upper set of points represents σ parameters, the lower set of points π parameters. Data points of the ground spin state structures (GS) and of structures with less stabilised multiplicities (ES) are colored black and blue, respectively. The error bars show the standard deviations resulting from sampled calculations. Labels indicate the metal with formal charge and multiplicity.

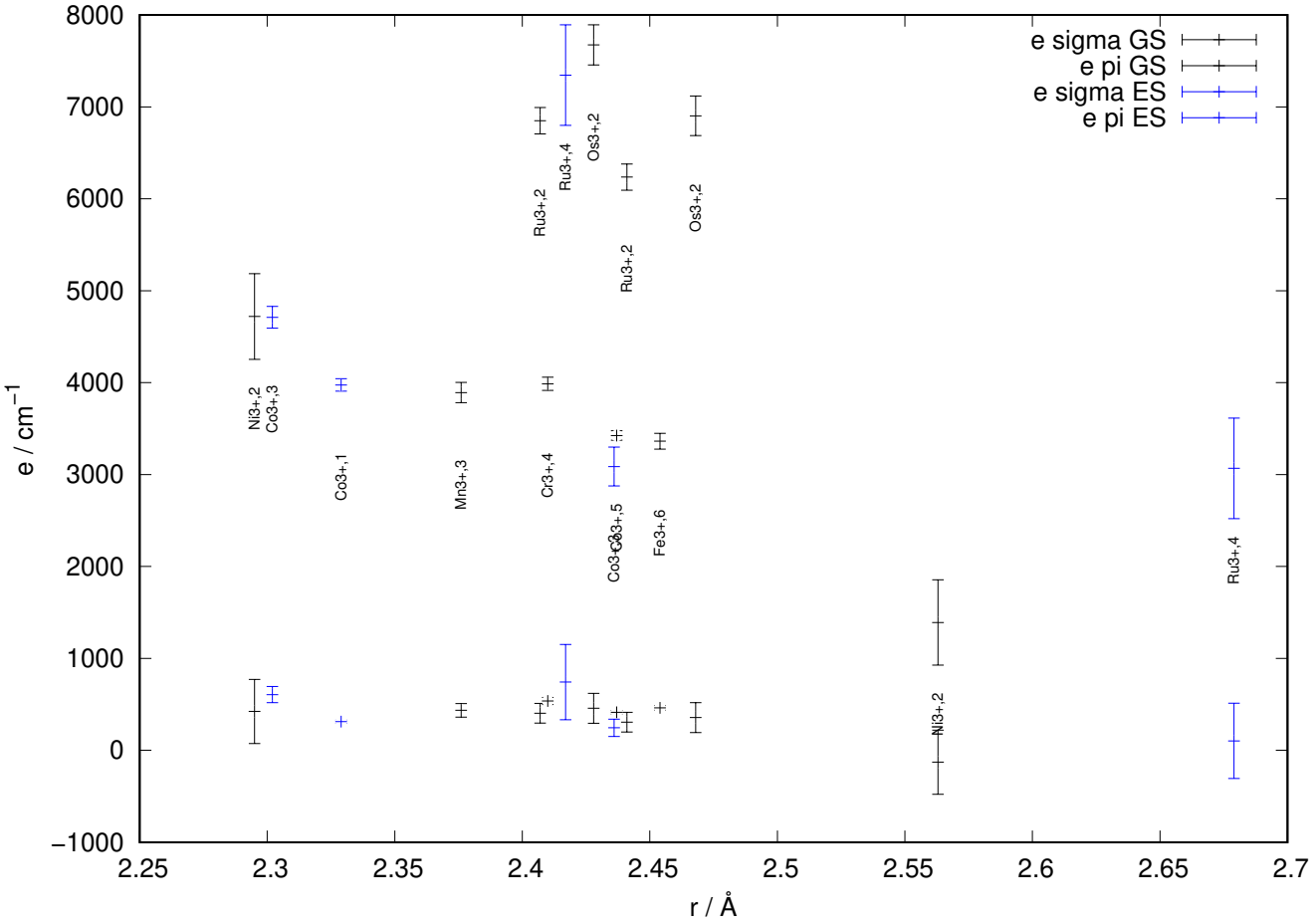

Figure 7: AOM parameters of M^{III} hexachloride complexes plotted versus the corresponding bond length. The upper set of points represents σ parameters, the lower set of points π parameters. Data points of the ground spin state structures (GS) and of structures with less stabilised multiplicities (ES) are colored black and blue, respectively. The error bars show the standard deviations resulting from sampled calculations. Labels indicate the metal with formal charge and multiplicity.

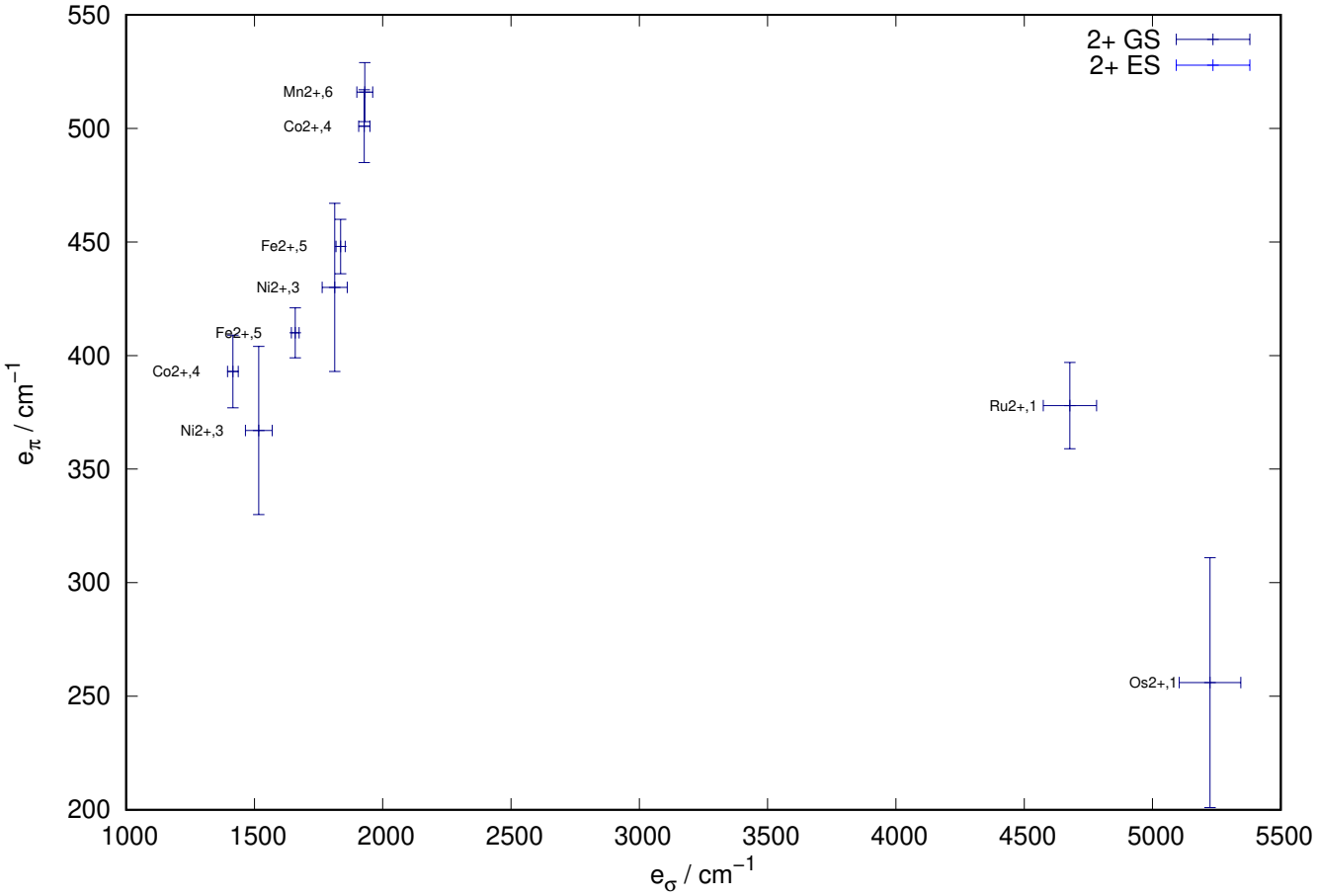

Figure 8: e_σ vs. e_π for M^{II} hexachloride complexes.

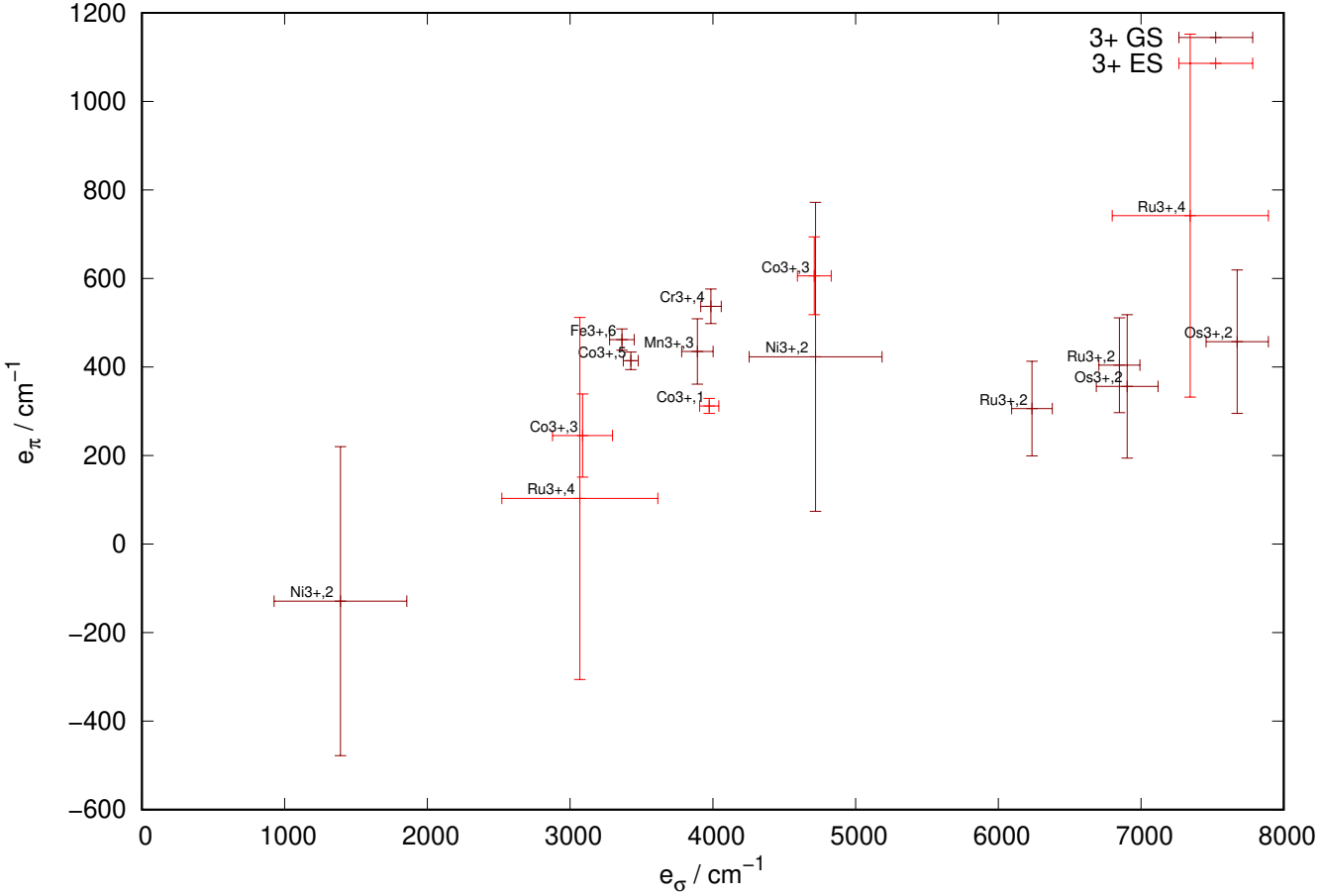

Figure 9: e_σ vs. e_π for M^{III} hexachloride complexes.

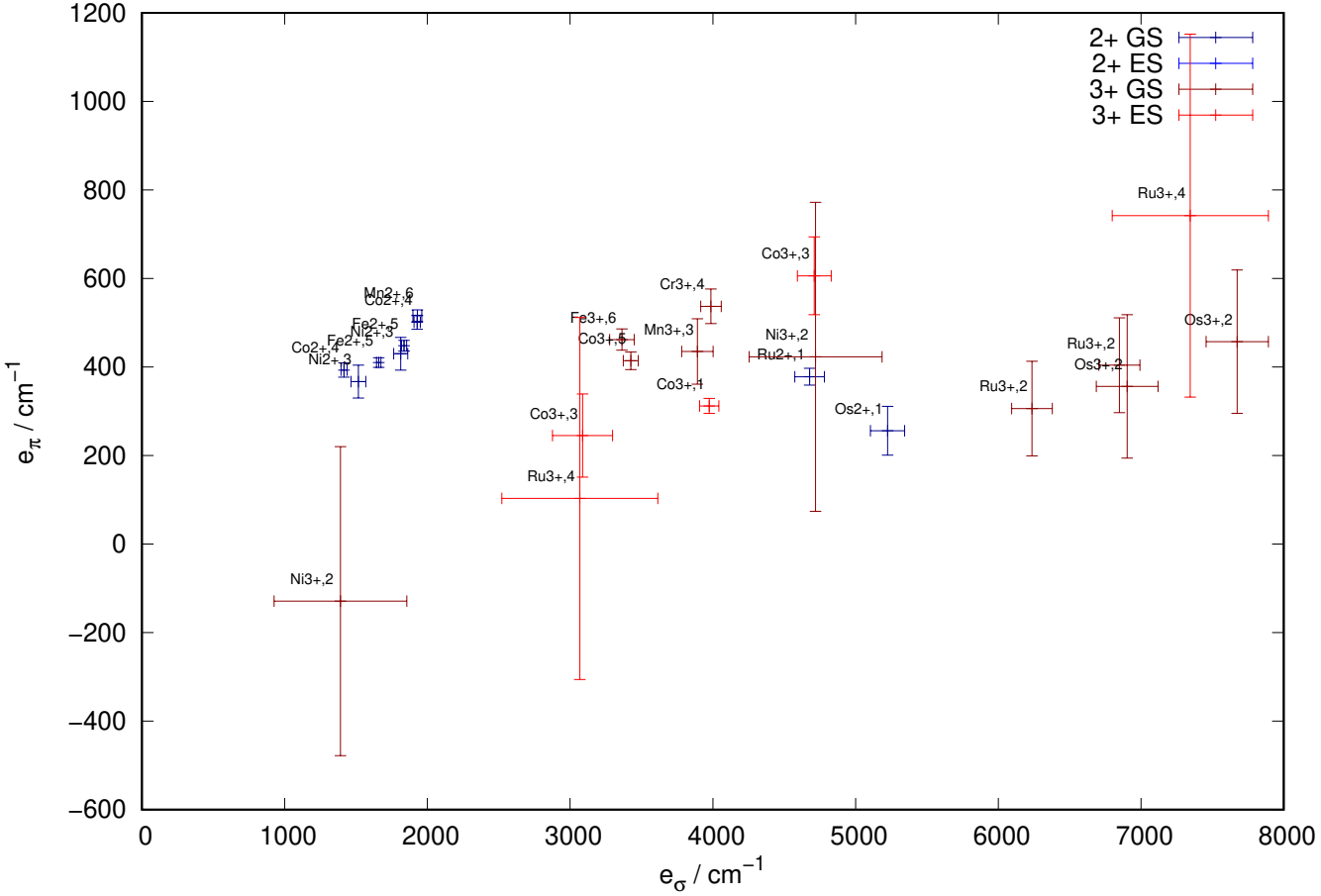

Figure 10: Plots 8 and 9 combined.

7 Table data for tetrammines

Table 8: AOM parameters for fictitious $[M(NH_3)_4]^{n+}$. Multiplicity refers to the multiplicity of the optimized ground state, ΔE ($kJ\,mol^{-1}$) is the energy difference of the given multiplicity to the ground state. If e_{ds} is not shown it was set to 0 in the fit. For shown e_{ds}, the molecule was oriented in the global axis frame for the CAS calculations.

Complex	$2S+1$	ΔE/kJ mol^{-1}	bond length / Å	e_σ/cm^{-1}	e_π/cm^{-1}	e_{ds}/cm^{-1}
$[Cr(NH_3)_4]^{2+}$	1	0	2.060(0.000)	6893(37)	1704(32)	
$[Mn(NH_3)_4]^{2+}$	6	0	2.191(0.000)	4723(113)	1343(85)	
$[Co(NH_3)_4]^{3+}$	5	43	2.073(0.001)	8800(111)	2620(106)	
$[Co(NH_3)_4]^{3+}$	3	0	2.000(0.000)	10166(29)	2449(18)	894(17)
$[Fe(NH_3)_4]^{3+}$	4	32	2.036(0.000)	9775(40)	2374(27)	966(13)
$[Fe(NH_3)_4]^{3+}$	6	0	2.103(0.001)	7101(474)	1614(361)	
$[Ni(NH_3)_4]^{3+}$	4	0	2.041(0.000)	8238(555)	1933(429)	

8 Table data for en and dien complexes

Table 9: AOM parameters for $[M(en)_3]^{n+}$.

Complex	$2S+1$	ΔE/kJ mol^{-1}		bond length / Å	e_σ/cm^{-1}	e_π/cm^{-1}
$[Cr(en)_3]^{2+}$	5	0	1	2.583(0.003)	1662(67)	270(45)
$[Cr(en)_3]^{2+}$	5	0	2	2.184(0.004)	5737(63)	822(48)
$[Cr(en)_3]^{2+}$	3	37	1	2.166(0.007)	4724(49)	-120(37)
$[Cr(en)_3]^{3+}$	4	0	1	2.141(0.000)	6010(48)	227(37)
$[Mn(en)_3]^{2+}$	6	0	1	2.344(0.000)	2517(11)	-106(8)
$[Mn(en)_3]^{3+}$	5	5	1	2.366(0.001)	2897(59)	71(43)
$[Mn(en)_3]^{3+}$	5	5	2	2.131(0.003)	6329(56)	588(43)
$[Mn(en)_3]^{3+}$	3	0	1	2.094(0.003)	5925(90)	106(66)
$[Fe(en)_3]^{2+}$	1	0	1	2.053(0.001)	3350(139)	-1097(105)
$[Fe(en)_3]^{2+}$	5	23	1	2.273(0.006)	2513(73)	-135(51)
$[Fe(en)_3]^{2+}$	3	53	1	2.253(0.000)	3430(58)	263(33)
$[Fe(en)_3]^{2+}$	3	53	2	2.225(0.001)	2099(62)	-514(26)
$[Fe(en)_3]^{2+}$	3	53	3	2.040(0.000)	4975(29)	145(22)
$[Fe(en)_3]^{3+}$	2	0	1	2.057(0.001)	6498(29)	450(21)
$[Fe(en)_3]^{3+}$	4	62	1	2.312(0.001)	2910(59)	-44(44)
$[Fe(en)_3]^{3+}$	4	62	2	2.087(0.010)	6331(58)	448(44)
$[Co(en)_3]^{2+}$	2	0	1	2.359(0.001)	1080(80)	-203(61)
$[Co(en)_3]^{2+}$	2	0	2	2.023(0.001)	5003(80)	267(60)
$[Co(en)_3]^{2+}$	4	6	1	2.224(0.001)	2946(14)	219(10)
$[Co(en)_3]^{3+}$	1	0	1	2.020(0.001)	5959(83)	-149(63)
$[Ni(en)_3]^{2+}$	3	0	1	2.177(0.000)	2556(52)	-75(39)
$[Ni(en)_3]^{3+}$	2	0	1	2.255(0.000)	3023(72)	-54(52)
$[Ni(en)_3]^{3+}$	2	0	2	2.018(0.002)	6968(71)	460(53)
$[Ru(en)_3]^{2+}$	1	0	1	2.161(0.001)	8489(83)	-542(62)
$[Ru(en)_3]^{3+}$	2	0	1	2.166(0.001)	11266(34)	587(29)
$[Os(en)_3]^{2+}$	1	0	1	2.180(0.001)	10466(76)	-487(57)
$[Os(en)_3]^{3+}$	2	0	1	2.184(0.002)	12880(48)	558(40)

Table 10: AOM parameters for $[M(dien)_2]^{n+}$.

Complex	$2S+1$	ΔE/kJ mol^{-1}		bond length / Å	e_σ/cm^{-1}	e_π/cm^{-1}
$[Cr(dien)_2]^{2+}$	5	0	1	2.389(0.026)	5446(151)	2012(114)
$[Cr(dien)_2]^{2+}$	5	0	2	2.149(0.000)	7772(132)	1968(96)
$[Cr(dien)_2]^{2+}$	3	42	1	2.177(0.010)	8206(687)	2588(519)
$[Cr(dien)_2]^{2+}$	3	42	2	2.122(0.003)	9018(642)	2387(475)
$[Cr(dien)_2]^{3+}$	4	0	1	2.140(0.020)	15264(291)	7054(230)
$[Mn(dien)_2]^{2+}$	6	0	1	2.346(0.020)	5280(98)	1896(143)
$[Mn(dien)_2]^{3+}$	5	0	1	2.276(0.010)	4515(292)	577(219)
$[Mn(dien)_2]^{3+}$	5	0	2	2.096(0.000)	7759(264)	968(192)
$[Mn(dien)_2]^{3+}$	3	11	1	2.095(0.020)	17034(1648)	8328(1233)
$[Fe(dien)_2]^{2+}$	5	20	1	2.302(0.008)	4660(230)	1646(174)
$[Fe(dien)_2]^{2+}$	5	20	2	2.237(0.000)	5251(200)	1455(146)
$[Fe(dien)_2]^{2+}$	3	46	1	2.251(0.025)	4838(90)	1515(67)
$[Fe(dien)_2]^{2+}$	3	46	2	2.027(0.000)	7412(79)	1668(66)
$[Fe(dien)_2]^{2+}$	1	0	1	2.049(0.019)	11295(1523)	4753(1135)
$[Fe(dien)_2]^{3+}$	2	0	1	2.056(0.017)	13350(866)	5482(618)
$[Fe(dien)_2]^{3+}$	4	47	1	2.091(0.035)	15444(355)	7041(266)
$[Fe(dien)_2]^{3+}$	4	47	2	2.315(0.019)	11931(371)	7053(274)
$[Fe(dien)_2]^{3+}$	6	62	1	2.240(0.002)	8525(77)	3239(60)
$[Fe(dien)_2]^{3+}$	6	62	2	2.304(0.001)	8014(65)	2586(46)
$[Co(dien)_2]^{2+}$	2	0	1	2.019(0.024)	10387(712)	4115(536)
$[Co(dien)_2]^{2+}$	2	0	2	2.395(0.070)	5965(747)	3819(554)
$[Co(dien)_2]^{2+}$	4	17	1	2.253(0.005)	5314(403)	2150(303)
$[Co(dien)_2]^{2+}$	4	17	2	2.183(0.010)	5901(359)	1985(270)
$[Co(dien)_2]^{3+}$	1	0	1	2.018(0.014)	17493(3624)	8398(2713)
$[Ni(dien)_2]^{2+}$	3	0	1	2.204(0.013)	5676(693)	2436(519)
$[Ni(dien)_2]^{2+}$	3	0	2	2.124(0.000)	6414(641)	2319(482)
$[Ni(dien)_2]^{3+}$	2	0	1	2.157(0.008)	3314(416)	-757(312)
$[Ni(dien)_2]^{3+}$	2	0	2	1.986(0.000)	6856(393)	-274(296)
$[Ru(dien)_2]^{2+}$	1	0	1	2.165(0.004)	17850(675)	6640(505)
$[Ru(dien)_2]^{2+}$	1	0	2	2.123(0.001)	18865(631)	6100(478)
$[Ru(dien)_2]^{3+}$	2	0	1	2.159(0.019)	21304(1207)	7859(899)
$[Os(dien)_2]^{2+}$	1	0	1	2.179(0.002)	21548(2241)	7998(1684)
$[Os(dien)_2]^{2+}$	1	0	2	2.144(0.000)	22417(2097)	7197(1570)
$[Os(dien)_2]^{3+}$	2	0	1	2.175(0.017)	23996(603)	8631(489)